Amidate Ligands for the Oxovanadium(IV) Cation: Design, Synthesis, Structure, and Spectroscopic and Electrochemical Properties

A. S. Borovik, Torin M. Dewey, and Kenneth N. Raymond*

Department of Chemistry, University of California at Berkeley, Berkeley, California 94720

Received June 29, 1992

With the goal of making vanadyl-specific ligands, the synthesis of a series of tetraanionic diamidate–diphenolate ligands and their respective oxovanadium(IV) complexes is reported. The strongly σ-donating ligands are constructed on a disubstituted propanediamide backbone, which stabilizes the highly oxidized vanadium(IV) center as evidenced by the remarkably low potential of –0.047 V (vs SCE) for the reversible VO^{3+}/VO^{2+} redox couple of the oxovanadium(IV) dianion complex. This potential can be varied over a ca. 0.50 V range upon 5-substitution of the phenolato ring with electron-donating or -withdrawing substituents (e.g., methyl, chloro, or nitro). The strongly σ-donating ligand environment provided by the diamidate–diphenolate ligands also results in relatively low $\nu_{V=O}$ of 942–955 cm^{-1} for the series of complexes and values of $10Dq$ of ca. 21 000 cm^{-1}. The structure of the potassium salt of [*N*,*N*′-bis(2-hydroxyphenyl)-2,2-diethylpropanediamido]oxovanadate(IV) is reported. The complex crystallizes in the space group $P\bar{1}$ with unit cell parameters of a = 13.577 (4) Å, b = 14.006 (4) Å, c = 15.933 (5) Å, α = 115.03 (2)°, β = 114.16 (3)°, γ = 90.37 (2)°, V = 2445 (4) Å^3, and Z = 4. Final residuals for the refinement of 556 variables against 4320 data were R = 5.3% and R_w = 7.0%. The structure contains two independent complex dianions which differ primarily in the conformation of the ethyl substituents of the propanediamide backbone and which exhibit the novel diamidate–diphenolate coordination to oxovanadium(IV).

We have begun a study to investigate the requisite factors for selective binding and stabilization of metal oxo cations. The ultimate goal is to develop molecular systems which will recognize these complex metal ions on the basis of their chemical and topological properties.[1] The approach we have taken is to synthesize receptor molecules which can covalently bind the metal ion center and interact with the oxo oxygen through an *intra*molecular hydrogen bond. Ideally, this ligand would be easily derivatized, allowing us to examine a variety of ligand types and hydrogen bond donors. In order to accomplish this task, we have designed a ligand system which contains two important components: (1) a tetradentate binding pocket that utilizes at least two amidate nitrogens

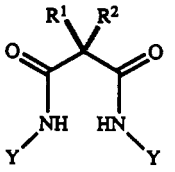

and (2) a propanediamide backbone which has pendant arms that can contain groups capable of hydrogen bonding to the oxygen moiety on the metal oxo cation.

Since the work of Margerum,[2] amidates have been known to stabilize highly oxidized metal ions. The recent structural examples of *N*-amidate coordination to oxomanganese(V),[3] oxovanadium(IV),[4] and dioxoosmium(VI)[5] further support the use of this donor group in the binding pocket design. Inspired by Collins' work on stabilizing high-valent metal ions,[6] we have designed a prototypical ligand H_4depa, which contains a di-*N*-amidate di-*O*-phenolate binding pocket.

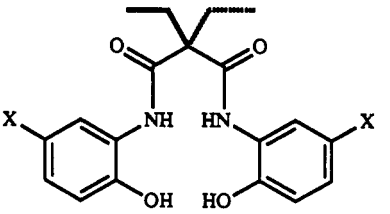

H_4depa-X

The development of a two point binding receptor necessitates that we understand how the individual bonding interactions affect the chemical properties of metal oxo cations. We have chosen to explore the coordination chemistry of the oxovanadium(IV) cation to delineate the covalent interactions associated with the metal oxo unit within the ligand framework. To probe the versatility of this molecular framework, we have examined the effects that a single substitution on the amidate–phenolate ring has on the electronic and redox properties of the metal oxo complexes. Therefore, a new series of ligands H_4depa-X, where X = H, Cl, Me, or NO_2 and $R^1 = R^2$ = Et has been synthesized. In this report we communicate the structural, electrochemical, and electronic properties of the oxovanadium(IV) complexes of these ligands.

Experimental Section

All reagents and solvents were purchased from commercial sources and used as received unless otherwise noted. The following solvents were distilled under nitrogen before use: tetrahydrofuran (THF)[7] from sodium

* Author to whom correspondence should be addressed.

(1) For an example of this approach applied to the sequestration of the uranyl ion, see: Franczyk, T. S.; Czerwinski, K. R.; Raymond, K. N. *J. Am. Chem. Soc.* **1992**, *114*, 8138.
(2) Margerum, D. W. *Pure Appl. Chem.* **1983**, *55*, 23 and references therein.
(3) (a) Collins, T. J.; Gordon-Wylie, S. W. *J. Am. Chem. Soc.* **1989**, *111*, 4511. (b) Collins, T. J.; Powell, R. D.; Slebodnick, C.; Uffelman, E. S. *J. Am. Chem. Soc.* **1990**, *112*, 89.
(4) Kabanos, T. A.; Kermidas, A. D.; Mentzafos, D.; Terzis, A. *J. Chem. Soc., Chem. Commun.* **1990**, 1664.
(5) Lin, J.-H.; Che, C.-M.; Lai, T.-F.; Poon, C.-K.; Cui, Y. X. *J. Chem. Soc., Chem. Commun.* **1991**, 468.
(6) Anson, F. C.; Collins, T. J.; Gipson, S. L.; Keech, J. T.; Krafft, T. E.; Peake, G. T. *J. Am. Chem. Soc.* **1986**, *108*, 6593.
(7) Abbreviations: TEA, triethylamine; SCE, saturated calomel electrode; cat, catecholate; salen, *N*,*N*′-ethylenebis(salicylideneaminate); acac, acetylacetonato; $TBAPF_6$, tetrabutylammonium hexafluorophosphate; H_2pycac, *N*-[2-(4-oxopentan-2-ylideneamino)phenyl]pyridine-2-carboxamide.

0020-1669/93/1332-0413$04.00/0

benzophenone ketyl; methanol and acetonitrile from CaH_2. Melting points were obtained with the use of a Buchi melting point apparatus and are uncorrected. Flash chromatography was performed according to the general procedure of Still.[8] Analytical thin-layer chromatography was done using Analtech silica gel GHLF glass-backed plates. Microanalyses were performed by the Microanalytical Laboratory at the University of California at Berkeley.

***N,N'*-Bis(2-hydroxyphenyl)-2,2-diethylpropanediamide (H_4depa-H).** Under an argon atmosphere, a mixture of 4.1 g (34 mmol) of *o*-anisidine and 6.2 g (61 mmol) of triethylamine in 100 mL of THF was stirred and cooled to 0 °C with an ice bath. After 15 min, the mixture was treated dropwise with 3.0 g (15 mmol) of diethyl malonyl dichloride. When the addition was completed, the mixture was allowed to warm to room temperature and then stirred an additional 2 h. This mixture was filtered and the filtrate concentrated under reduced pressure. The residue was dissolved in 75 mL of ethyl acetate and extracted with two 50-mL portions of 1 M HCl, 50 mL of water, and 50 mL of brine, and dried over Na_2SO_4. The solvent was evaporated under reduced pressure, and 4.7 g (83%) of the dimethyl-protected ligand was obtained as white solid, which was used without further purification. This compound was suspended in 20 mL of argon-saturated CH_2Cl_2 and treated with 6.1 mL of neat BBr_3. After 24 h, the solution was carefully poured into 200 mL of water and the CH_2Cl_2 was boiled off. The resulting white solid was collected on a coarse fritted glass funnel, washed with 3 portions of water, and dried under vacuum to afford 3.4 g (92%) of the product. ^{1}H NMR: δ 0.86 (t, J = 7.2 Hz, 6H, $-CH_2-CH_3$), 2.04 (q, J = 7.2 Hz, 4H, $-CH_2-CH_3$), 6.77 (td, J = 7.6, 1.5 Hz, 2H, C_5–*H* of Ar), 6.86 (dd, J = 8.0, 1.5 Hz, 2H, C_3–*H* of Ar), 6.96 (td, J = 7.0, 1.5, 2H, C_4–*H* of Ar), 7.76 (dd, J = 8.0, 1.4, 2H, C_6–*H* of Ar), 9.75 (s, 2H, ArO*H*), 10.06 (s, 2H, ArN*H*CO).

***N,N'*-Bis(5-chloro-2-hydroxyphenyl)-2,2-diethylpropanediamide (H_4depa-Cl).** This compound was prepared as described for H_4depa-H with the following modifications. The dimethyl-protected product was obtained as a white solid by flash chromatography using 1:2 ethyl acetate/hexanes as the eluent (R_f = 0.3) and then recrystallization from CH_2Cl_2/cyclohexane (78%). The pure product H_4depa-Cl was isolated as a white solid in 98% yield. ^{1}H NMR: δ 0.84 (t, J = 7.2 Hz, 6H, $-CH_2-CH_3$), 2.05 (q, J = 7.2 Hz, 4H, $-CH_2-CH_3$), 6.88 (d, J = 8.6 Hz, 2H, C_3–*H* of Ar), 7.02 (dd, J = 8.5, 2.3 Hz, 2H, C_4–*H* of Ar), 7.86 (d, J = 2.3, 2H, C_6–*H* of Ar), 10.18 (s, 2H, ArO*H*), 10.21 (s, 2H, ArN*H*CO).

***N,N'*-Bis(2-hydroxy-5-methylphenyl)-2,2-diethylpropanediamide (H_4depa-Me).** This compound was prepared by following the same procedure outlined for H_4depa-H. The dimethyl-protected product was isolated in 80% yield after recrystallization from CH_2Cl_2/cyclohexane. Pure H_4depa-Me was obtained as a gray powder in 94% yield. ^{1}H NMR: δ 0.91 (t, J = 7.2 Hz, 6H, $-CH_2-CH_3$), 2.09 (q, J = 7.2 Hz, 4H, $-CH_2-CH_3$), 6.81 (s, 4H, C_3–*H* and C_4–*H* of Ar), 7.87 (s, 2H, C_6–*H* of Ar), 9.55 (s, 2H, ArO*H*), 10.06 (s, 2H, ArN*H*CO).

***N,N'*-Bis(2-hydroxy-5-nitrophenyl)-2,2-diethylpropanediamide (H_4depa-NO_2).** This compound was prepared as described for H_4depa-H. The following modifications were employed in the synthesis of the dimethyl-protected ligand. To prevent deprotonation of the amide nitrogens, two additional equivalents of 2-methoxy-5-nitroaniline were substituted for triethylamine during the synthesis. Methylene chloride was added to the organic layer during the workup to ensure all the product was dissolved. The protected ligand was isolated as a brownish-yellow powder in 34% yield, while the product H_4depa-NO_2 was obtained in 40% yield as a yellow solid. ^{1}H NMR: δ 0.86 (t, J = 7.2 Hz, 6H, $-CH_2-CH_3$), 2.04 (q, J = 7.2 Hz, 4H, $-CH_2-CH_3$), 7.05 (d, J = 9.0 Hz, 2H, C_3–*H* of Ar), 7.98 (dd, J = 9.1, 2.9 Hz, 2H, C_4–*H* of Ar), 8.74 (d, J = 2.8, 2H, C_6–*H* of Ar), 10.46 (s, 2H, ArO*H*), 10.56 (s, 2H, ArN*H*CO).

Tetrabutylammonium [*N,N'*-Bis(2-hydroxyphenyl)-2,2-diethylpropanediamido]oxovanadate(IV) ($(Bu_4N)_2$[VO(depa-H)]). A stirred solution of 0.25 g (0.73 mmol) of H_4depa-H in N_2-saturated methanol was treated with 0.95 g (15 mmol) of 40% (wt) tetrabutylammonium hydroxide in water and stirred for 15 min. In one portion, solid $VO(acac)_2$ (0.19 g, 0.73 mmol) was then added to this solution. After 4 h of heating at ca. 40 °C, all volatiles were removed under reduced pressure and the green residue was dried under vacuum overnight. The complex was purified on a Sephadex (LH-20) chromatography column using methanol as the eluent. A dark green band was obtained, which afforded 0.57 g (88%) of a green solid after drying under vacuum for 18 h. Anal. Calcd (found) for $[C_{51}H_{90}N_4O_5V]\cdot 0.5CH_3OH$: C, 68.26 (68.17); H, 10.23 (10.16); N, 6.18 (5.84); V, 5.62 (5.60).

(8) Still, W. C.; Kahn, M.; Mitra, A. *J. Org. Chem.* **1978**, *43*, 2923.

Tetrabutylammonium [*N,N'*-Bis(5-chloro-2-hydroxyphenyl)-2,2-diethylpropanediamido]oxovanadate(IV) ($(Bu_4N)_2$[VO(depa-Cl)]). The compound was prepared as described for $(Bu_4N)_2$[VO(depa-H)] to give 0.46 g (82%) of a green solid. Anal. Calcd (found) for $[C_{51}H_{88}Cl_2N_4O_5V]\cdot 1.0CH_3OH$: C, 63.00 (63.10); H, 9.37 (9.39); N, 5.65 (5.63).

Tetrabutylammonium [*N,N'*-Bis(2-hydroxy-5-methylphenyl)-2,2-diethylpropanediamido]oxovanadate(IV) ($(Bu_4N)_2$[VO(depa-Me)]). This complex was synthesized by following the same procedure outlined for $(Bu_4N)_2$[VO(depa-H)]. The complex was isolated as a green solid. Yield: 0.62 g (92%). Anal. Calcd (found) for $[C_{53}H_{94}N_4O_5V]\cdot 1.0CH_3OH$: C, 68.29 (68.09); H, 10.39 (10.22); N, 5.90 (5.70); V, 5.36 (5.15).

Tetrabutylammonium [*N,N'*-Bis(5-nitro-2-hydroxyphenyl)-2,2-diethylpropanediamido]oxovanadate(IV) ($(Bu_4N)_2$[VO(depa-NO_2)]). This compound was isolated as a yellow-brown solid by the protocol for $(Bu_4N)_2$[VO(depa-H)]. Anal. Calcd (found) for $[C_{51}H_{88}N_6O_9V]\cdot 2.0H_2O$: C, 60.28 (60.08); H, 9.12 (9.46); N, 8.27 (8.36).

Physical Methods. ^{1}H NMR spectra were obtained at 250 MHz on a superconducting FT spectrometer constructed at UC Berkeley, equipped with a Cryomagnets, Inc., magnet and a Nicolet Model 1280 data collection system. All samples were run in d_6-DMSO and are reported in parts per million (ppm) relative to an internal standard of Me_4Si. EPR spectra were obtained at X-band with an IBM ER-200D-SCR spectrometer. Samples were prepared in chloroform ($\sim 10^{-3}$ M) and recorded at room temperature.

Visible spectra of the complexes in methanol were obtained using either a Hewlett-Packard 8450A diode array or a Perkin-Elmer Lambda 9 spectrophotometer. A 0.10-cm quartz cell was used to minimize solvent absorption. IR spectra were recorded on a Nicolet 5DXB FTIR spectrometer and are reported in wavenumbers. Samples were prepared in mineral oil and run on KBr plates. Electrochemical studies were performed with a BAS 100A (Bioanalytical Systems Inc., West Lafayette, IN). All experiments were done under nitrogen at ambient temperature in acetonitrile solution with 0.1 M tetrabutylammonium hexafluorophosphate as the supporting electrolyte. The acetonitrile was obtained from Burdick-Jackson Laboratories and used without further purification. Cyclic voltammograms (CV) were obtained by using a three-component system consisting of a glassy-carbon disk working electrode, a platinum wire auxiliary electrode, and a BAS saturated calomel reference electrode (SCE) containing a Vycor plug to separate it from the bulk. IR compensation was achieved before each CV was recorded. The ferrocenium/ferrocene couple was used to monitor the reference electrode and was observed at +415 mV. Controlled-potential coulometry (CPC) was performed employing a three-compartment cell with each chamber separated by a coarse glass frit. The sample compartment was fitted with a Teflon stir bar, a Teflon-hose N_2 inlet, and a platinum-mesh working electrode. The other compartments housed either a platinum wire auxiliary electrode or a Ag/AgCl reference electrode containing a Vycor plug. The end point of the titration was determined when the current of the cell reached the background current. The mass of each sample was measured with a Cahn 4400 electrobalance.

X-ray Crystallographic Determination of K_2[VO(depa-H)]·1.5CH_3CN·1.0H_2O. K_2[VO(depa-H)] was prepared as described above using ethanolic KOH instead of tetrabutylammonium hydroxide. Clear light-green blocklike crystals of the potassium salt of the complex were obtained by slow diffusion of ether into an acetonitrile solution of the complex. A crystal of dimensions 0.22 × 0.31 × 0.35 mm was cut from a larger block and was mounted on the end of a capillary using Paratone N hydrocarbon oil and transferred to an Enraf-Nonius CAD-4 diffractometer. The crystal was cooled to −111 °C under a stream of cold N_2. Crystal data, together with the details of the diffraction experiment, are listed in Table I. The cell constants were determined by least-squares refinement of 24 strong, high-angle ($\theta \geq 10.8°$) reflections well-spaced throughout reciprocal space. Automated indexing procedures yielded a triclinic unit cell, and inspection of the cell constants revealed no conventional cell of higher symmetry. Inspection of the cell volume indicated that two crystallographically independent complexes were present in the unit cell (Z = 4). Orientation and intensity control reflections were monitored every 200 reflections and every 1 h of data collection, respectively. Azimuthal (ψ) scans were recorded for three strong reflection with $\chi > 80°$ at the end of the data collection. Lorentz and polarization corrections were applied to the data, and an absorption correction based on the ψ scans was applied to the data (transmission 0.91–1.00).

The structure was solved using the SHELXS-86 direct methods program,[9] which revealed the presence of two independent complex anions

Table I. Summary of Crystallographic Data and Parameters for $K_2[VO(depa\text{-}H)]\cdot 0.75CH_3CN\cdot 0.4H_2O$

molecular formula	$C_{20.5}H_{20.25}N_{2.75}O_{5.2}VK_2$
fw	517.49
temp (K)	162
cryst system	triclinic
space group (No.)	$P\bar{1}$ (2)
cell constants[a]	
a (Å)	13.577 (4)
b (Å)	14.006 (4)
c (Å)	15.933 (5)
α (deg)	115.03 (2)
β (deg)	114.16 (3)
γ (deg)	90.37 (2)
Z	4
V (Å^3)	2445 (4)
abs coeff, μ_{calc} (cm^{-1})	7.66
δ_{calc} (g/cm^3)	1.410
$F(000)$	1064
cryst dimens (mm)	0.22 × 0.31 × 0.35
radiation	Mo Kα (λ = 0.710 73)
diffractometer	Enraf-Nonius CAD-4
h,k,l ranges collcd	0→14, -15→15, -17→15
2θ range	$3° \le 2\theta \le 45°$
scan type	ω–2θ
scan speed (θ, deg/min)	5.61
no. of reflcns collcd	6388
no. of unique reflcns	6388
no. of reflcns with $F_o^2 > 3\sigma(F_o^2)$	4320
no. of params	556
data/param ratio	7.8
$R = [\sum\|\Delta F\|/\sum\|F_o\|]$	0.053
$R_w = [\sum w(\Delta F)^2/\sum wF_o^2]$	0.070
GOF	1.537
final diff $\rho_{max}{}^+$ (e/Å^3)	+1.48[b]

[a] Unit cell parameters and their esd's were derived by a least-squares fitting of the setting angles of 24 reflections in the range $21.6° \le 2\theta \le 24.9°$. [b] Located near O11 (solvent oxygen).

and four potassium counterions and confirmed the choice of the centric space group $P\bar{1}$ (No. 2). Subsequent iterations of least-squares refinement and difference Fourier calculations revealed the presence of 1.5 acetonitriles of solvation and one solvent water oxygen, in addition to some ill-defined solvent structure near the solvent oxygen (O11), per asymmetric unit. The structure was refined using standard least-squares and Fourier techniques with the MOLEN package.[10] Hydrogen atoms on the ligands were included in the structure factor calculations in the final cycles of refinement at calculated positions 0.95 Å from, and with values of B_{iso} 1.25 times that of, the carbon atom to which they were attached. The p-factor, used to reduce the weight of intense reflections, was set to 0.07 for the final cycles of refinement. The 20 worst reflections were zero-weighted in the final cycles of refinement, and the final residuals for 556 variables refined against the 4320 data for which $F_o^2 > 3\sigma(F_o^2)$ were R = 5.3%, R_w = 7.0%, and GOF = 1.537. The R value for all data was 8.5%. The largest peak in the final difference Fourier map of +1.48 e/Å^3 was situated near O11.

The positional and B_{eqv} thermal parameters of the non-hydrogen atoms are given in Table II. Anisotropic thermal parameters and the positions and thermal parameters of the hydrogen atoms are available as supplementary material.

Results and Discussion

Design Considerations and Syntheses. The H_4depa-X ligands were designed to stabilize the highly oxidized metal centers in oxometal cations. Their tetraanionic binding pocket provides strong σ-bond donation to the metal through di[*N*-amidate–*O*-phenolate] coordination. These ligands differ from other diamidate–diphenol ligands[6] in several ways. First, upon metal coordination one six- and two five-member metallocycles are formed. These chelate rings are important because they provide rigidity to the metal complex. In particular, the six-membered ring formed with the propanediamide moiety gives a platform from which to append hydrogen bond donors. Second, alkylation at the methylene carbon of the propanediamide backbone increases the resistance of the ligand to oxidation. In the H_4depa-X series

Table II. Positional Parameters for Non-Hydrogen Atoms in $\{K_2[VO(depa\text{-}H)]\}_2\cdot 1.5CH_3CN\cdot 0.75H_2O$

atom	x	y	z	B(iso),[a] Å^2
V1	0.07514 (8)	0.74177 (7)	0.22740 (6)	1.91 (2)
V2	0.16145 (9)	0.20276 (8)	0.14968 (7)	2.49 (3)
K1	0.0887 (1)	0.40406 (9)	0.04907 (8)	2.39 (3)
K2	–0.0028 (1)	0.0397 (1)	–0.11136 (8)	3.09 (4)
K3	–0.0261 (1)	–0.0141 (1)	0.34582 (9)	3.10 (4)
K4	0.3983 (1)	0.5361 (1)	0.38890 (9)	2.85 (4)
O1	0.0721 (3)	0.8545 (3)	0.2226 (3)	2.8 (1)
O2	–0.0729 (3)	0.6519 (3)	0.1400 (3)	2.7 (1)
O3	0.1120 (3)	0.6382 (3)	0.1218 (2)	2.2 (1)
O4	0.0591 (3)	0.8994 (3)	0.4969 (3)	3.0 (1)
O5	0.3398 (3)	0.7200 (3)	0.4619 (3)	2.7 (1)
O6	0.1488 (4)	0.0736 (3)	0.0844 (3)	3.1 (1)
O7	0.0259 (3)	0.2316 (3)	0.0661 (2)	2.4 (1)
O8	0.2352 (3)	0.2824 (3)	0.1099 (3)	3.1 (1)
O9	0.0675 (3)	0.1334 (3)	0.3258 (3)	2.9 (1)
O10	0.4015 (3)	0.3749 (3)	0.4552 (3)	3.0 (1)
O11	–0.1909 (6)	0.9255 (6)	0.1413 (5)	7.0 (2)
N1	0.0292 (4)	0.7639 (3)	0.3392 (3)	2.0 (1)
N2	0.2287 (4)	0.7450 (3)	0.3226 (3)	1.9 (1)
N3	0.0840 (4)	0.2211 (3)	0.2374 (3)	2.2 (1)
N4	0.3072 (4)	0.2651 (3)	0.2798 (3)	2.3 (1)
N5	–0.592 (2)	1.013 (2)	–0.126 (2)	15.2 (9)*
N6	–0.1507 (4)	0.5130 (4)	–0.2737 (4)	3.8 (1)*
C1	0.2644 (5)	0.7597 (4)	0.4212 (4)	2.3 (2)
C2	0.2186 (5)	0.8394 (4)	0.4872 (4)	2.1 (1)
C3	0.0946 (5)	0.8355 (4)	0.4402 (4)	2.3 (1)
C4	0.2764 (6)	0.9545 (5)	0.5182 (5)	3.4 (2)
C5	0.3980 (6)	0.9801 (6)	0.5701 (6)	5.1 (3)
C6	0.2465 (6)	0.8266 (5)	0.5856 (4)	3.5 (2)
C7	0.1800 (6)	0.7261 (5)	0.5633 (4)	4.6 (2)
C8	–0.1385 (5)	0.6810 (5)	0.1859 (4)	2.7 (2)
C9	–0.0874 (5)	0.7444 (4)	0.2960 (4)	2.1 (1)
C10	–0.1545 (5)	0.7766 (5)	0.3451 (4)	3.1 (2)
C11	–0.2675 (5)	0.7482 (6)	0.2901 (5)	4.2 (2)
C12	–0.3168 (6)	0.6849 (6)	0.1824 (5)	4.6 (2)
C13	–0.2538 (5)	0.6511 (6)	0.1310 (4)	3.6 (2)
C14	0.2884 (5)	0.6958 (4)	0.2660 (4)	2.3 (1)
C15	0.2220 (5)	0.6427 (4)	0.1569 (4)	2.1 (1)
C16	0.2687 (5)	0.5967 (5)	0.0906 (4)	2.5 (2)
C17	0.3807 (5)	0.6006 (5)	0.1313 (4)	3.2 (2)
C18	0.4470 (5)	0.6536 (6)	0.2370 (5)	3.6 (2)
C19	0.4012 (5)	0.7012 (5)	0.3030 (4)	3.0 (2)
C20	0.3221 (5)	0.3010 (4)	0.3784 (4)	2.4 (2)
C21	0.2448 (5)	0.2430 (4)	0.3974 (4)	2.7 (2)
C22	0.1248 (5)	0.1928 (4)	0.3149 (4)	2.5 (2)
C23	0.2343 (6)	0.3254 (5)	0.4959 (4)	3.7 (2)
C24	0.1744 (6)	0.4104 (6)	0.4831 (5)	4.6 (2)
C25	0.3004 (6)	0.1569 (5)	0.4232 (5)	4.0 (2)
C26	0.3130 (6)	0.0678 (5)	0.3365 (6)	5.2 (2)
C27	–0.0303 (5)	0.2147 (4)	0.1823 (4)	2.3 (2)
C28	–0.0571 (5)	0.2251 (4)	0.0913 (4)	2.4 (2)
C29	–0.1627 (5)	0.2321 (5)	0.0337 (4)	3.2 (2)
C30	–0.2418 (5)	0.2294 (6)	0.0659 (5)	4.0 (2)
C31	–0.2181 (5)	0.2173 (5)	0.1533 (5)	3.8 (2)
C32	–0.1129 (5)	0.2087 (5)	0.2100 (4)	3.1 (2)
C33	0.3902 (5)	0.3016 (4)	0.2607 (4)	2.4 (2)
C34	0.3475 (5)	0.3108 (5)	0.1686 (4)	3.0 (2)
C35	0.4183 (6)	0.3461 (6)	0.1410 (5)	4.7 (2)
C36	0.5298 (6)	0.3703 (6)	0.2011 (5)	4.9 (2)
C37	0.5728 (5)	0.3584 (6)	0.2895 (5)	3.9 (2)
C38	0.5040 (5)	0.3246 (5)	0.3199 (4)	3.0 (2)
C40	–0.417 (2)	0.965 (2)	–0.114 (1)	7.8 (5)*
C41	–0.515 (2)	0.981 (2)	–0.124 (1)	7.4 (5)*
C42	0.0359 (6)	0.5065 (6)	0.7171 (5)	5.1 (2)*
C43	–0.0702 (5)	0.5097 (5)	–0.2764 (4)	3.2 (1)*

[a] An asterisk indicates a thermal parameter for an isotropically refined atom. The thermal parameter given for anisotropically refined atoms is the isotropic equivalent thermal parameter defined as $(4/3)[a^2{*}B(1,1) + b^2B(2,2) + c^2{}_B(3,3) + ab(\cos\gamma)B(1,2) + ac(\cos\beta)B(1,3) + bc(\cos\alpha)B(2,3)]$, where a, b, and c are real cell parameters and $B(i,j)$ values are anisotropic β's.

(9) Sheldrick, G. *Crystallographic Computing 3*; Oxford University Press: Oxford, U.K., 1985.
(10) *Molen Structure Determination Package*; Enraf-Nonius: Delft, The Netherlands, 1991.

Scheme I [a]

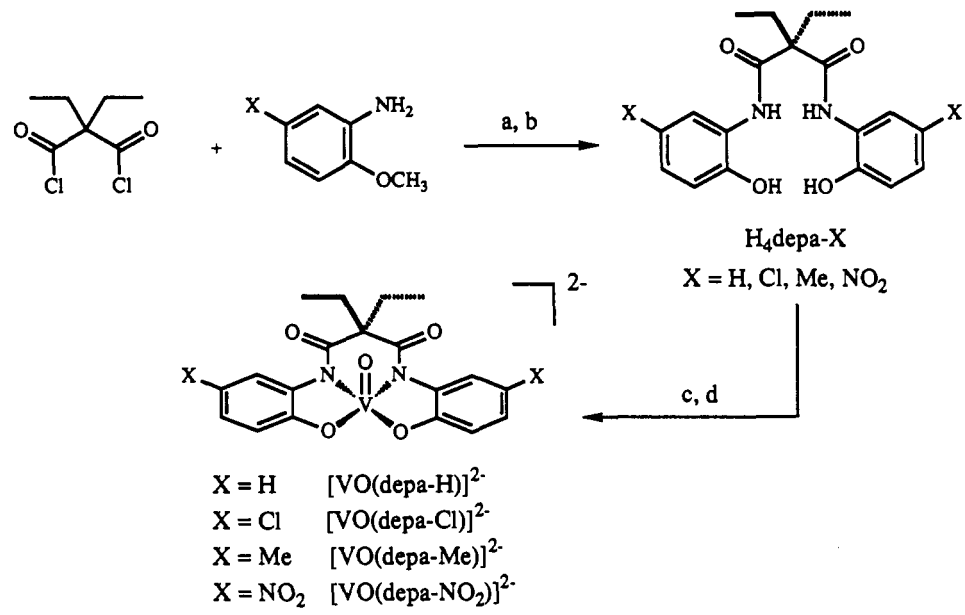

[a] Key: (a) TEA/THF/0 °C; (b) BBr_3/CH_2Cl_2; (c) Bu_4NOH/MeOH; (d) $VO(acac)_2$.

this methylene group is "protected" with ethyl substituents. Third, the ease of substitution at this position allows us to examine a variety of different hydrogen bond donors. Finally, various groups can be placed about the aryl rings of the binding pocket to tune the physical properties of the metal complexes.

The new diamidate–diphenolate ligands H_4depa-X (where X = H, Cl, Me, NO_2) and their corresponding oxovanadium(IV) complexes were synthesized as outlined in Scheme I. Treatment of the appropriate methoxyaniline with diethyl malonyl dichloride afforded the dimethyl-protected ligand in high yield. Conversion to the diamide–diphenol ligand was cleanly accomplished with BBr_3 in methylene chloride. The oxovanadium(IV) complexes were readily obtained by allowing a methanolic solution of $[H_2depa]^{2-}$ to react with $VO(acac)_2$. The isolation of the complexes was not hindered by the presence of dioxygen or water.

The $[VO(depa-X)]^{2-}$ complexes are resistant to oxidative or hydrolytic decomposition. The complexes were manipulated without any precautions to exclude dioxygen or water. In the solid state these complexes are stable indefinitely, while in solution they exist for weeks. This is in sharp contrast to other five-coordinate, dianionic VO^{2+} complexes which tend to be oxygen and/or water sensitive. For example, bis(catecholate)-derived oxovanadium(IV) complexes are only stable under anaerobic conditions, in both solution *and* the solid state.[11] The stability of these complexes is undoubtedly coupled to the strong donor ability of the *N*-amidate–*O*-phenolate binding pocket and the resistance of the H_4depa-X ligands to oxidation (vide infra). The $[VO(depa-X)]^{2-}$ complexes thus offer a further illustration on how *N*-amidate donors can be utilized in stabilizing highly oxidized metal centers.

Description of the Solid-State Structure of $\{K_2[VO(depa-H)]\}_2 \cdot 1.5CH_3CN \cdot H_2O$. The H_4depa-X ligands are precursors of molecular systems that can act as metal oxo cation receptors. An important aspect of the present work is to examine the structural characteristics of $[VO(depa-X)]^{2-}$ complexes to be used as a reference in the future design and construction of ligands with hydrogen-bonding appendages. To this end, the solid-state structure of $K_2[VO(depa-H)]$ was determined by single-crystal X-ray diffraction. This structure apparently also represents the first example of di(*N*-amidate–*O*-phenolate) coordination to a metal oxo cation. Selected distances and angles for the structure are shown in Table III. Other distances and angles for the complex anions are provided as supplementary material.

The $VO[depa-H]^{2-}$ structure is composed of two crystallographically independent oxovanadium dianionic compounds, denoted $[VO(depa-H)_a]^{2-}$ and $[VO(depa-H)_b]^{2-}$, which are linked by a network of potassium counterions and solvent molecules. The potassium counterions are coordinated by combinations of phenolate oxygens, ligand carbonyl oxygens, and solvent heteroatoms (Figures 1 and 2). The two independent metal complexes differ primarily in the conformation of the propanediamide backbone and the orientation of the ethyl arms (vide infra). In each of the two complexes the vanadyl ion is coordinated in the equatorial plane forming square-based pyramidal coordination around the vanadium. This geometry is borne out by comparing the two *trans*-O_{eq}–V–N_{eq} angles for each complex. For square pyramidal VO^{2+} structures these angles are approximately 140–145°, whereas a coordination geometry that was distorted toward trigonal bipyramidal coordination would have the two unique trans angles diverge toward 120 and 180° (for idealized D_{3h} symmetry).[12] The two trans angles are 142.4 (2)°/145.1 (2)° for $[VO(depa-H)_a]^{2-}$ and 142.5 (2)°/146.4 (2)° for complex $[VO(depa-H)_b]^{2-}$. The vanadium atoms lie 0.615 and 0.602 Å out of the plane of the four equatorial donors, with the two O_{eq}–V–N_{eq} planes of the two bidentate donors defining dihedral angles with each other of 131.6° ($[VO(depa-H)_a]^{2-}$) and 132.3° ($[VO(depa-H)_b]^{2-}$). These dihedral angles are similar to those found in the similar bis(catecholate)-containing oxovanadium(IV) complexes. The planes defined by the two phenolato–amido rings on each complex generate dihedral angles of 171.5° for $[VO(depa-H)_a]^{2-}$ and 162.4° for $[VO(depa-H)_b]^{2-}$, exhibiting how the phenyl rings are bent slightly down and away from VO^{2+}.

The vanadyl V–O distances are 1.613 (5) and 1.625 (4) Å for the two complexes, within the range expected for oxovanadium(IV) complexes.[13] These distances are somewhat longer than

(11) Cooper, S. R.; Koh, Y. B.; Raymond, K. N. *J. Am. Chem. Soc.* **1982**, *104*, 5092.

(12) Determined for all square pyramidal oxovanadium structures using the Cambridge Structural Database QUEST91 program, constraining the O(oxo)–V–L_{eq} angles to between 85 and 115°. For idealized C_{4v} square pyramidal structures, these angles would be 151.9°: (a) Muetterties, E. L.; Guggenberger, L. J. *J. Am. Chem. Soc.* **1974**, *96*, 1748. (b) Orioli, P. L. *Coord. Chem. Rev.* **1971**, *6*, 285.

(13) The solid-state IR spectrum of the $K_2[VO(depa-H)]$ compound shows two intense absorptions at 953 and ca. 940 cm^{-1} (sh), which are assigned as $\nu_{V=O}$ for the independent $[VO(depa-H)_a]^{2-}$ and $[VO(depa-H)_b]^{2-}$ complex anions.

Table III. Selected Distances (Å) and Angles (deg) for $\{K_2[VO(depa\text{-}H)]\}_2 \cdot 1.5CH_3CN \cdot 0.75H_2O$

	$K_2[VO(depa\text{-}H)_a]$ distances		
V1–O1	1.613 (5)	C2–C6	1.546 (10)
V1–O2	1.938 (3)	C4–C5	1.469 (10)
V1–O3	1.953 (4)	C6–C7	1.490 (11)
V1–N1	2.026 (6)	C8–C9	1.423 (7)
V1–N2	2.001 (4)	C8–C13	1.396 (8)
O2–C8	1.334 (9)	C9–C10	1.391 (10)
O3–C15	1.355 (7)	C10–C11	1.370 (8)
O4–C3	1.236 (8)	C11–C12	1.394 (9)
O5–C1	1.243 (7)	C12–C13	1.370 (12)
N1–C3	1.355 (5)	C14–C15	1.414 (6)
N1–C9	1.414 (7)	C14–C19	1.385 (9)
N2–C1	1.359 (8)	C15–C16	1.381 (9)
N2–C14	1.423 (9)	C16–C17	1.378 (9)
C1–C2	1.513 (9)	C17–C18	1.375 (7)
C2–C3	1.527 (8)	C18–C19	1.373 (11)
C2–C4	1.566 (9)		
	$K_2[VO(depa\text{-}H)_b]$ Distances		
V2–O6	1.625 (4)	C21–C25	1.539 (10)
V2–O7	1.944 (4)	C23–C24	1.484 (11)
V2–O8	1.937 (5)	C25–C26	1.494 (10)
V2–N3	2.007 (6)	C27–C28	1.415 (9)
V2–N4	2.016 (4)	C27–C32	1.377 (11)
O7–C28	1.356 (9)	C28–C29	1.381 (8)
O8–C34	1.366 (7)	C29–C30	1.373 (12)
O9–C22	1.245 (9)	C30–C31	1.380 (12)
O10–C20	1.251 (5)	C31–C32	1.381 (9)
N3–C22	1.358 (8)	C33–C34	1.404 (10)
N3–C27	1.416 (7)	C33–C38	1.387 (8)
N4–C20	1.353 (8)	C34–C35	1.374 (12)
N4–C33	1.424 (10)	C35–C36	1.362 (9)
C20–C21	1.520 (11)	C36–C37	1.372 (12)
C21–C22	1.525 (7)	C37–C38	1.374 (13)
C21–C23	1.571 (9)		
	$K_2[VO(depa\text{-}H)_a]$ Angles		
O1–V1–O2	108.17 (20)	V1–O2–C8	112.3 (3)
O1–V1–O3	110.87 (22)	V1–O3–C15	113.0 (3)
O1–V1–N1	103.91 (22)	V1–N1–C3	121.2 (5)
O1–V1–N2	109.41 (19)	V1–N1–C9	109.4 (3)
O2–V1–O3	85.49 (16)	V1–N2–C1	125.9 (5)
O2–V1–N1	80.86 (17)	V1–N2–C14	111.1 (3)
O2–V1–N2	142.41 (21)	O5–C1–N2	123.2 (6)
O3–V1–N1	145.09 (20)	O5–C1–C2	119.3 (5)
O3–V1–N2	82.16 (16)	N2–C1–C2	117.0 (5)
N1–V1–N2	89.35 (20)	C1–C2–C3	119.1 (4)
	$K_2[VO(depa\text{-}H)_b]$ Angles		
O6–V2–O7	104.06 (16)	V2–O7–C28	114.0 (4)
O6–V2–O8	111.04 (23)	V2–O8–C34	113.1 (4)
O6–V2–N3	106.32 (24)	V2–N3–C22	119.8 (4)
O6–V2–N4	109.50 (20)	V2–N3–C27	111.5 (4)
O7–V2–O8	85.94 (19)	V2–N4–C20	126.5 (5)
O7–V2–N3	81.63 (20)	V2–N4–C33	110.1 (3)
O7–V2–N4	146.44 (17)	O10–C20–N4	122.6 (7)
O8–V2–N3	142.46 (18)	O10–C20–C21	118.5 (5)
O8–V2–N4	82.03 (20)	N4–C20–C21	118.6 (4)
N3–V2–N4	89.11 (20)	C20–C21–C22	119.5 (5)

seen in most oxovanadium(IV) complexes, e.g. VO(salen),[14] where the V=O distance is 1.584 (4) Å. They are similar, however to the V=O distance of 1.613 (5) Å seen in the bis(catecholato)-oxovanadium(IV) complex[11] and to other bis(catecholamido)-oxovanadium(IV) complexes where four anionic equatorial donor ligands are present.[15] The average $V-O_{eq}$ distances are 1.946 (4) and 1.941 (5) Å for the two complexes, typical for negatively charged oxygen donors. The average $V-N_{eq}$ distances are slightly longer, at 2.013 (5) and 2.012 (5) Å, consistent with the slightly larger radius of nitrogen, and within the range of V–N distances seen in the literature. The only other known vanadium(IV)–amidate N distance is 1.984 (2) Å.[4,16]

There is significant strain in the six-member metallocycle formed between the vanadium(IV) ion and the propanediamido backbone. This strain is exhibited by the increase in the C1–C2–C3 and C20–C21–C22 angles from idealized 109.5 to 119.1 (5) and 119.6 (5)° for the two independent anions (Table III and also Figure 1]). The average angles around the central carbon of the propanediamido backbone to the ethyl arms are only slightly distorted, at 108.0 (5) and 108.1 (6)° for the complexes $[VO(depa\text{-}H)_a]^{2-}$ and $[VO(depa\text{-}H)_b]^{2-}$, respectively. The remaining angles of the propanediamide backbone are unexceptional, and the amide carbonyl shows no significant distortion from the opening up of the ligand backbone. The geometry around the amidate nitrogens and the phenyl rings is unexceptional. Comparisons of the C(aryl)–N, N–C(carbonyl), and intra-ring distances to crystallographically characterized *N*-aryl amides show no significant shifts attributable to complexation to the vanadium center.

Although the complexes have similar metal coordination environments, $[VO(depa\text{-}H)_a]^{2-}$ and $[VO(depa\text{-}H)_b]^{2-}$ differ in the conformations of their propanediamido backbones and diethyl appendages (Figure 1). One ethyl arm on complex $[VO(depa\text{-}H)_a]^{2-}$ (C6–C7) is oriented below the plane of equatorial coordination, opposite from the vanadyl oxygen, whereas the other ethyl arm (C4–C5) has the methyl carbon (C5) oriented away from the vanadyl oxygen. In contrast, both ethyl groups on $[VO(depa\text{-}H)_b]^{2-}$ are swung inward, toward the vanadium coordination sphere. Also, the two carbonyl groups on the backbone of the ligand are oriented up and down in the opposite manner for each of the complexes, so that the six-membered chelate rings are in a "twist-boat" type of conformation. This results in a twisting of the coordinated amides away from planarity.

Twisting the amides out of plane should decrease the delocalization of the nitrogen lone pairs onto the carbonyl oxygen and may result in stronger σ-donation to the oxovanadium(IV) center.[17] The deformation from planarity for the amide functions can be described using parameters as described by Dunitz and Winkler[18] and modified by Collins,[17] so that the degree of twist is expressed as the parameter $\bar{\tau}$, which provides an approximate measure of the angle between the nitrogen and carbonyl carbon π orbitals. The carbon–nitrogen pπ overlap should be close to zero for $\bar{\tau} = \pm 90°$, and $\bar{\tau} = 0°$ for idealized cisoid or transoid geometries. The $\bar{\tau}$ values for the amide groups in both complexes are $\bar{\tau} = 24$ and 27° for complex $[VO(depa\text{-}H)_a]^{2-}$ and $\bar{\tau} = -38$ and −22° for complex $[VO(depa\text{-}H)_b]^{2-}$. These values clearly indicate that the coordinated amides are distorted from planarity, although not to the same degree as some of Collins' compounds, which show $\bar{\tau}$ values between 46 and 73°.[19,20]

Infrared Spectroscopy. We have used the V=O stretching frequency to gauge the donor strength of the $(depa\text{-}X)^{4-}$ ligands.

(14) (a) Pasquali, M.; Marchetti, F.; Floriani, C.; Cesari, M. *Inorg. Chem.* **1980**, *19*, 1198. (b) Riley, P. E.; Pecoraro, V. L.; Carrano, C. J.; Bonadies, J. A.; Raymond, K. N. *Inorg. Chem.* **1986**, *25*, 154.

(15) Dewey, T. M.; Du Bois, J.; Raymond, K. N. Unpublished results.

(16) The vanadium(IV)–amidate N distance seen in the VO(pycac) complex in ref 3 is significantly shorter than seen in the $[VO(depa\text{-}H)]^{2-}$ complex described herein and is the shortest known V–N distance for oxovanadium(IV). We can speculate that this is due to the weaker, dianionic ligand set in Kabanos' complex, which results in a higher effective charge on the vanadium center and shorter V–N distances. However, the discrepancy could also be ascribed to ligand constraints within either of the complexes.

(17) (a) Collins, T. J.; Coots, R. J.; Furutani, T. T.; Keech, J. T.; Peake, G. T.; Santarsiero, B. D. *J. Am. Chem. Soc.* **1986**, *108*, 5333. (b) Anson, F. C.; Collins, T. J.; Gipson, S. L.; Keech, J. T.; Krafft, T. E.; Peake, G. T. *J. Am. Chem. Soc.* **1986**, *108*, 6593.

(18) (a) Dunitz, J. D.; Winkler, F. K. *J. Mol. Biol.* **1971**, *59*, 169. (b) Dunitz, J. D.; Winkler, F. K. *Acta Crystallogr., Sect. B: Struct. Crystallogr. Cryst. Chem.* **1975**, *B13*, 251.

(19) Although these compounds are constrained to have the amidate–phenolate groups twisted out of the equatorial plane of coordination, resulting in very twisted amide functions.

(20) The solid-state IR spectrum for $K_2[VO(depa\text{-}H)]$ shows two broad peaks at ca. 1590 cm^{-1}. These features are consistent with there being unsymmetrical carbonyl groups of the coordinated amido in the two independent anions.

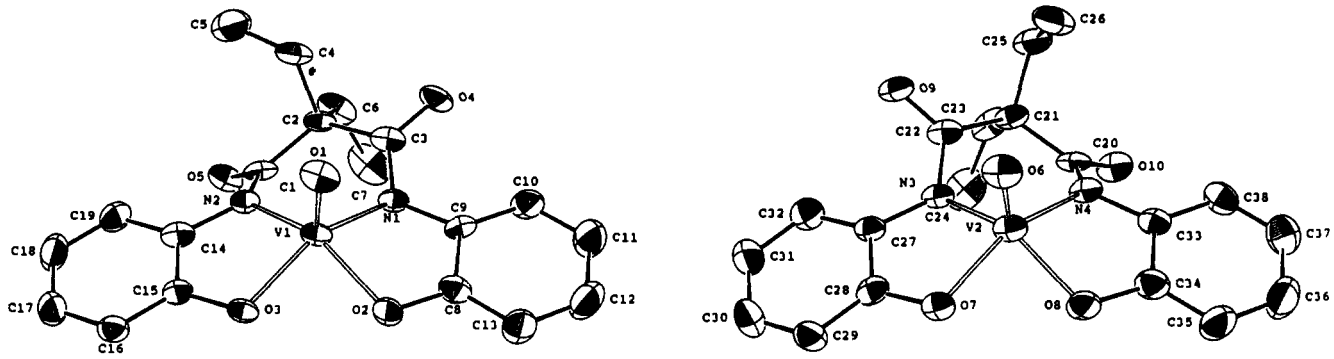

Figure 1. ORTEP diagrams of the two crystallographically independent complex dianions $[VO(depa\text{-}H)_a]^{2-}$ (left) and $[VO(depa\text{-}H)_b]^{2-}$ (right). Ellipsoids are drawn at the 50% probability level.

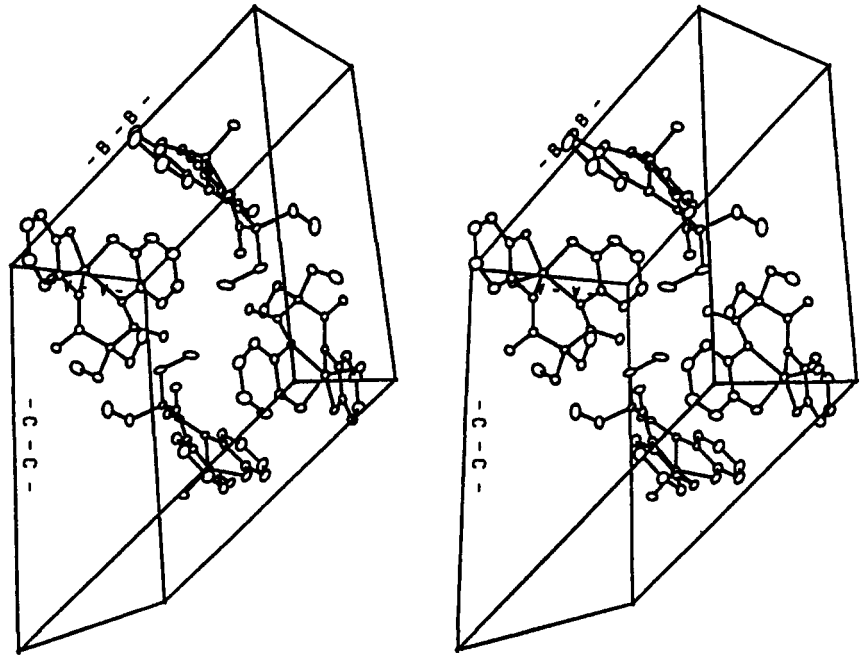

Figure 2. Stereoscopic view of the unit cell packing diagram for $K_2[VO(depa\text{-}H)]\cdot 0.75CH_3CN\cdot 0.5H_2O$. The top and bottom complexes are $[VO(depa\text{-}H)_a]^{2-}$ and the left and right complexes are $[VO(depa\text{-}H)_b]^{2-}$. The solvent atoms and potassium counterions are removed for clarity.

The multiple bond character of the oxygen–vanadium interaction is affected by the Lewis basicity of the ancillary ligands bound to the vanadium. Increasing the electron density at the vanadium through ligand coordination causes a reduction in the amount of $p\pi_{(oxo)} \rightarrow d\pi_{(V)}$ donation from the multiply bonded oxygen. The decrease in the oxygen–vanadium bond order is reflected in a lowering of $\nu_{V=O}$.[21] As shown in Table IV, the V=O stretching frequencies for the $(Bu_4N)_2[VO(depa\text{-}X)]$ complexes range from 942 to 955 cm^{-1}. These values are significantly lower than those found for other five-coordinate VO^{2+} complexes (1100–960 cm^{-1}).[21] For example, bis(catecholato)oxovanadium(IV) complexes have V=O stretching frequencies between 975 and 960 cm^{-1},[11] whereas those of five-coordinate, neutral Schiff base VO^{2+} complexes occur at ca. 980 cm^{-1}.[14b,22,23] Moreover, the $\nu_{V=O}$ values of the $[VO(depa\text{-}X)]^{2-}$ complexes are comparable to those found for six-coordinate oxovanadium complexes that have ligands trans to the oxo.[23] This lowering of $\nu_{V=O}$ in the $[VO(depa\text{-}X)]^{2-}$ complexes is another indication of the strong σ bonding of the equatorial coordinated di[*N*-amidate–*O*-phenolate] ligands. The resultant decrease of the oxygen–vanadium bond order effects an increase in the basicity of the oxo oxygen, which is important for our design of receptors that will intramolecularly hydrogen bond (vide supra).

(21) Selbin, J.; Holmes, L. H.; McGlynn, S. P. *J. Inorg. Nucl. Chem.* **1963**, *25*, 1359.
(22) Li, X.; Lah, M. S.; Pecoraro, V. L. *Inorg. Chem.* **1988**, *27*, 4657.
(23) Bonadies, J. A.; Carrano, C. J. *J. Am. Chem. Soc.* **1986**, *108*, 4088.

Table IV. Summary of Spectral Data for $[VO(depa\text{-}X)]^{2-}$ and Related Complexes

complex	λ, nm (ε, M^{-1} cm^{-1})[a]	$\nu_{V=O}$, cm^{-1}	⟨*g*⟩ (⟨*A*⟩, 10^{-4} cm^{-1})[c]	ref
$[VO(depa\text{-}H)]^{2-}$	610 (27), 481 (sh), 294 (12 400)	945[b]	2.00 (83)	*d*
$[VO(depa\text{-}Me)]^{2-}$	613 (26), 480 (sh), 300 (13 500)	942[b]	2.00 (83)	*d*
$[VO(depa\text{-}Cl)]^{2-}$	608 (35), 478 (30), 309 (13 500)	947[b]	2.00 (83)	*d*
$[VO(depa\text{-}NO_2)]^{2-}$	580 (sh), 404 (19000), 318 (sh), 280 (25 800)	955[b]	2.00 (83)	*d*
$[VO(cat)_2]^{2-}$	656 (69), 540 (sh)[e]	970[f]	1.977 (82)[e]	11
$[VO(DTBC)]^{2-}$	654 (150)[g]	977[f]	1.970 (77)[g]	11
VO(salen)	592 (180)[c,h]	981[f]	1.974 (93)[i]	22
$[VO(EHPG)]^-$	540 (160)[h]	979[f]	1.984 (86)[a]	22

[a] In MeOH. [b] IR spectra of the TBA salts were recorded as Nujol mulls on KBr plates. [c] In $CHCl_3$ at room temperature. [d] This work. [e] In H_2O (0.1 M KOH). [f] KBr pellet. [g] In EtOH. [h] $b_2 \rightarrow b_1$ transition. [i] In DMF.

Electronic Absorption Properties. Calculations and spectroscopic data for oxovanadium(IV) complexes indicate the relative energies of the d orbitals are $d_{xy} < d_{xz},d_{yz} < d_{x^2-y^2} < d_{z^2}$ (or $b_2 < e < b_1 < a_1$ in C_{4v} symmetry, with equatorial ligands in the *xz* and *yz* planes).[24,25] The d–d bands found in square pyramidal VO^{2+} complexes thus correspond to the $b_2 \rightarrow e$, $b_2 \rightarrow b_1$, and $b_2 \rightarrow a_1$ transitions. Only the first two transitions are usually observed because the $b_2 \rightarrow a_1$ transition is obscured by more

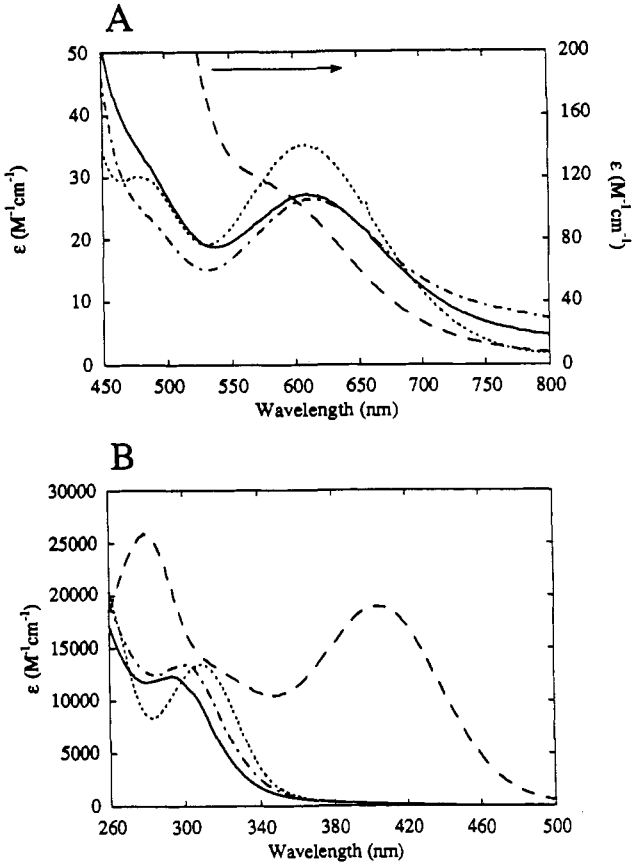

Figure 3. (A) Visible and (B) UV–visible spectra of $[VO(depa-X)]^{2-}$ in methanol: (—) X = H; (- · -) X = Me; (- · -) X = Cl; (– – –) X = NO_2.

intense charge-transfer and/or ligand-based transitions. In addition, Ballhausen and Gray showed that the $b_2 \rightarrow b_1$ transition is a direct measure of $10Dq$.[24a]

The absorption data for the $(Bu_4N)_2[VO(depa-X)]$ complexes are found in Table IV, and their visible spectra in methanol are displayed in Figure 3. The spectra of $[VO(depa-H)]^{2-}$, $[VO(depa-Me)]^{2-}$, and $[VO(depa-Cl)]^{2-}$ exhibit two features: a broad band centered at 610 nm ($\epsilon \sim 30\ M^{-1}\ cm^{-1}$) and a shoulder at 470–480 nm. The low- and high-energy components are assigned as the $b_2 \rightarrow e$ and $b_2 \rightarrow b_1$ transitions, respectively.[26] The visible absorption spectrum of $[VO(depa-NO_2)]^{2-}$ is dominated by an intense band at 404 nm ($\epsilon = 18\ 600\ M^{-1}\ cm^{-1}$) that arises from the $(depa-NO_2)^{4-}$ ligand. Additionally, there is a low-energy shoulder at 580 nm that is assigned as $b_2 \rightarrow e$. The band at 404 nm prevents the observation of the other metal-centered transitions.

Included in Table IV are the spectroscopic properties of several other oxovanadium(IV) complexes. The data reveal that the $b_2 \rightarrow e$ and $b_2 \rightarrow b_1$ transitions for the $[VO(depa-X)]^{2-}$ complexes occur at higher energies compared to those of other VO^{2+} complexes. The value of $10Dq$ is ca. 21 000 cm^{-1} for $[VO(depa-X)]^{2-}$ (for X = H, Me, Cl), significantly larger than other five-coordinate oxovanadium(IV) complexes (e.g. $10Dq$ = 18 500 cm^{-1} for $[VO(cat)_2]^{2-}$).[11] The magnitude of $10Dq$ can be explained by examining the orbitals involved in the $b_2 \rightarrow b_1$ transition. The b_2 (d_{xy}) orbital is nonbonding whereas the b_1 ($d_{x^2-y^2}$) orbital is influenced greatly by the equatorial ligands because it has σ^* ($V-L_{eq}$) character. Strong equatorial σ-donors would increase the relative energy of the b_1 orbital and cause a blue shift in the $b_2 \rightarrow b_1$ transition. The strong ligand-field character of the $(depa-X)^{4-}$ ligands is further evidence that di[*N*-amidate–*O*-phenolate] coordination provides an electron-rich environment about the vanadium.

Table V. Electrochemical Properties of the $[VO(depa-X)]^{2-}$ Complexes[a]

$[VO(depa-X)]^{2-}$ X	$E^{\circ\prime}$ [b]	ΔE_p [b,c]	i_c/i_a [c]	$E_{p,a}^{ox2}$ [b]
H	–0.047	68	1.01	0.85
Me	–0.095	68	1.01	0.78
Cl	0.105	66	1.00	1.00
NO_2	0.399	66	1.10	1.30

[a] In CH_3CN. [b] Unit of V vs SCE. [c] ΔE_p = 0.062 V and i_c/i_a = 1.01 for the Fc^+/Fc couple under the same experimental conditions.

EPR Spectroscopy. In $CHCl_3$ at room temperature the $[VO(depa-X)]^{2-}$ complexes have characteristic eight-line EPR spectra of the d^1 oxovanadium(IV) moiety. The signals are centered at $\langle g \rangle = 2.00$, with isotopic hyperfine splitting constants of 83 cm^{-1} (Table IV). The g values are slightly higher than those found for most VO^{2+} complexes (1.91–2.0),[24] indicating that the energy levels are somewhat farther apart. These results agree with the other spectroscopic measurements in suggesting that the d_{xz}, d_{yz} (e) and $d_{x^2-y^2}$ (b_1) orbitals are at relatively higher energies than the d_{xy} (b_2) orbital because of the strong σ donation from the equatorial bound $(depa-X)^{4-}$ ligands.

Electrochemistry. We have investigated the redox properties of the $[VO(depa-X)]^{2-}$ complexes by cyclic voltammetry and controlled-potential coulometry. The results for the cyclic voltammetric experiments are presented in Table V. Between 0.50 and –0.50 V in CH_3CN $[VO(depa-H)]^{2-}$ exhibits a one-electron redox wave at –0.047 V versus SCE, which is assigned to the VO^{3+}/VO^{2+} couple (Figure 4B). This redox process approaches reversibility as measured by (1) the value for ΔE_p being ~0.068 V, (2) the $E^{\circ\prime}$ value being independent of scan rate from 0.050 to 1.00 V/s, and (3) the current of the cathodic and anodic waves being equal ($i_c/i_a \sim 1.0$). In addition, plots of peak current versus $V^{1/2}$ between 0.050 and 1.00 V/s are linear for this couple, indicating that it is a diffusion-controlled process. The $E^{\circ\prime}$ value of the VO^{3+}/VO^{2+} couple for $[VO(depa-H)]^{2-}$ occurs at a substantially more negative potential when compared to other five-coordinate oxovanadium(IV) complexes. For example, the corresponding couple in VO(salen) occurs at 0.47 V,[27] which is over 0.50 V more positive than $E^{\circ\prime}$ for $[VO(depa-H)]^{2-}$. In fact, these $E^{\circ\prime}$ values indicate that the VO^{3+} species is favored thermodynamically by 48 kJ/mol in the $[VO(depa-H)]^-$ complex as compared to the VO^{3+} species in the $[VO(salen)]^+$ complex. The low potential and near reversibility of this couple further illustrates the ability of the $(depa-X)^{4-}$ ligands to stabilize highly oxidized metal ion centers.

Also included in Figure 4 are the cyclic voltammograms (CV) of the other $[VO(depa-X)]^{2-}$ complexes. All the complexes have quasi-reversible one-electron waves similar to that found for $[VO(depa-H)]^{2-}$. Substitution at the 5-position on the amidato–phenolato rings has a profound effect on the VO^{3+}/VO^{2+} potentials for this isostructural series of complexes. The electrochemical potentials of the $[VO(depa-X)]^{2-}$ complexes span ca. 0.50 V, corresponding to an energy difference of 47 kJ/mol. The change in redox potential has a linear correlation with the Hammett σ constants (R = 0.997 for the linearly regressed line) and yields

(24) (a) Ballhausen, C. J.; Gray, H. B. *Inorg. Chem.* **1962**, *1*, 111. (b) Selbin, J. *Chem. Rev.* **1965**, *2*, 153. (c) Vanquickenborne, L. G.; McGlynn, S. P. *Theoret. Chim. Acta (Berl.)* **1968**, *9*, 390. (d) Deeth, R. J. *J. Chem. Soc., Dalton Trans.* **1991**, 1467.

(25) There has been some controversy about the ordering of the d orbitals.[21b] Specifically, the problem is in the relative energies of the e and b_1 orbitals. Their ordering depends on the balance between the σ-donor strength of the equatorial ligands and the V–O π bonding. For the $VO(depa-X)]^{2-}$ complexes, the equatorial coordination of the di[*N*-amidate–*O*-phenolate] ligands causes the $d_{x^2-y^2}$ (b_1) orbital to be at higher in energy than that of the d_{xz},d_{yz} (e) orbitals.

(26) We are assuming that the spectroscopic site symmetry is close to C_{4v} for the $[VO(depa-X)]^{2-}$ complexes.

(27) Bonadies, J. A.; Bulter, W. M.; Pecoraro, V. L.; Carrano, C. J. *Inorg. Chem.* **1987**, *26*, 1218.

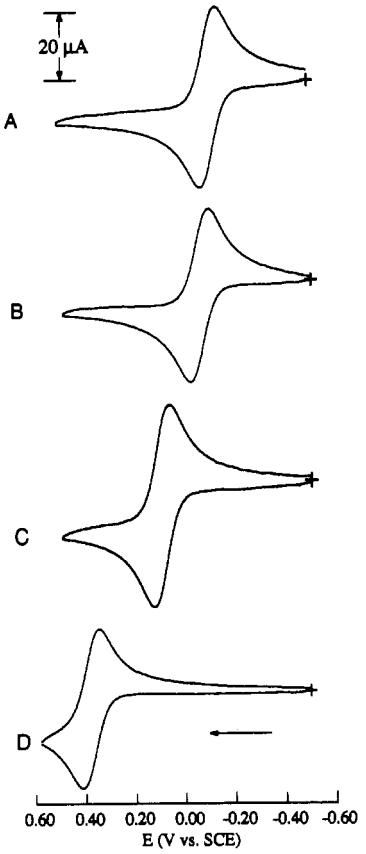

Figure 4. Cyclic voltammograms for $[VO(depa-X)]^{2-}$ versus SCE in CH_3CN with 0.1 M $TBAPF_6$ under N_2 at a 0.100 V/s scan rate: (A) X = Me; (B) X = H; (C) X = Cl; (D) X = NO_2. All cyclic voltammograms were initiated at E = –0.500 V versus SCE.

a ρ of 9.09.[28,29] An increase in the electron-withdrawing capacity of the substituent will decrease the basicity (and σ-donor strength) of the $(depa-X)^{4-}$ ligands. This causes a lowering in energy of the d-orbital manifold and therefore makes it more difficult to oxidize the oxovanadium(IV) complexes. The electronic effect on the VO^{3+}/VO^{2+} potentials is amplified because all four donor atoms bound to the vanadium(IV) center from the $(depa-X)^{4-}$ ligands are influenced by the substitution on the amidato–phenolato rings. This amplified effect is reflected in the large value for ρ obtained from the Hammett analysis and the broad range in electrochemical potentials observed for the $[VO(depa-X)]^{2-}$ complexes.[30]

Controlled-potential coulometry (CPC) was employed to further explore the VO^{3+}/VO^{2+} couple in $[VO(depa-H)]^{2-}$. At a potential of 0.400 V versus SCE, CPC experiments measured 0.97 e^-/mol of $[VO(depa-H)]^{2-}$, which agrees with the assignment of this redox couple being a one-electron oxidation. In addition, the oxidized solution from the CPC experiment has similar cyclic voltammetric properties as the starting $[VO(depa-H)]^{2-}$ solution. This suggests that the oxidized species is stable under the conditions of the CPC experiment. Upon oxidation, the color of the solution changes from light Celtic green to a dark blue-green. The intense blue-green color (λ_{max} = 865 nm; $\epsilon \sim 3300$ M^{-1} cm^{-1}) of the oxidized solution most likely arises from a ligand-to-metal charge-transfer (LMCT) transition from the bound phenolates to vanadium(V). This type of LMCT transition has been seen before in a variety of VO^{3+} complexes that have phenolates coordinated to the vanadium(V) center.[23,31] The oxidized product $[VO(depa-H)]^-$ has been chemically synthesized and has the same visible spectrum as the oxidized solution obtained by CPC,[32] thus supporting the association of the 865-nm band with the VO^{3+} species.

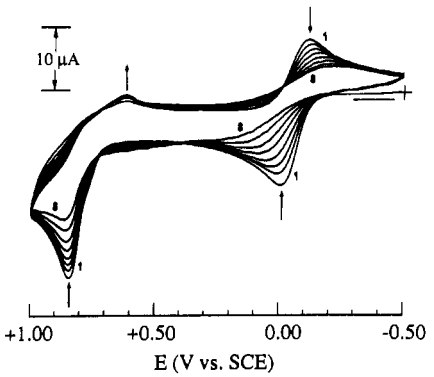

Figure 5. Cyclic voltammograms of $[VO(depa-H)]^{2-}$ showing the effects of repeated scanning (traces 1–8) between +1.0 and –0.50 V versus SCE. Scan 1 was started at E = –0.500 V versus SCE.

The $[VO(depa-X)]^{2-}$ complexes have a second, irreversible oxidative wave between 0.75 and 1.4 V. The potential of this oxidative wave ($E_{p,a}^{ox2}$) depends on the 5-substituent of the amidato–phenolato ring, moving to higher potentials with more electron-withdrawing substituents (Table V), and is attributed to a ligand-centered process.[33] Cyclic voltammetric experiments suggest that only $[VO(depa-NO_2)]^{2-}$ is stable to oxidation past 0.75 V. For $[VO(depa-H)]^{2-}$, scanning anodically past $E_{p,a}^{ox2}$ to 1.0 V and then cathodically to –0.50 V produces ~15% loss in the cathodic current of the VO^{3+}/VO^{2+} couple. This oxidative instability is illustrated in Figure 5 for $[VO(depa-H)]^{2-}$, where CVs obtained by repetitive scanning from –0.50 to 1.00 V show a sequential drop in anodic and cathodic current for both the VO^{3+}/VO^{2+} couple and $E_{p,a}^{ox2}$. The $[VO(depa-Cl)]^{2-}$ and $[VO(depa-Me)]^{2-}$ complexes are more stable than $[VO(depa-H)]^{2-}$, but they too show decomposition upon repeated scans past their corresponding $E_{p,a}^{ox2}$. The oxidation that occurs at $E_{p,a}^{ox2}$ clearly affects the overall stability of the oxovanadium complexes. While the identity of this oxidized species is unknown, it is plausible that the second oxidation initially produces a semiquinone-like species. This oxidized compound could then either dissociate from VO^{3+} or be involved in further chemical processes.[34,35]

The stabilization of a highly oxidized metal center, such as VO^{3+}, requires a strongly basic ligand—which in turn will tend to be easily oxidized. Hence, a ligand structure is necessary that manages to be a strong base but a poor reducing agent. In the $[VO(depa-X)]^{2-}$ series the complex with X = NO_2 is the least basic ligand and is the most resistant to oxidation ($E_{p,a}^{ox2} > 1.25$ V), whereas $[VO(depa-Me)]^{2-}$ is the complex with the most basic ligand, and both the VO^{3+}/VO^{2+} couple ($E^{o\prime}$ = –0.100) and the

(28) Lowry, T. H.; Richardson, K. S. *Mechanism and Theory in Organic Chemistry*; Harper & Row: New York, 1981.
(29) A similar value for ρ (7.35) has been observed for a series of Mn(III)/Mn(II) Schiff base complexes: Gohdes, J. Ph.D. Dissertation, University of California, Berkeley, CA, 1991.
(30) Collins has recently reported that a series of tetraamidate manganyl complexes have a linear correlation for a redox couple versus Hammett σ^+ values, with a ρ of –27 (Workman, J. M.; Powell, R. D.; Procyk, A. D.; Collins, T. J.; Bocian, D. F. *Inorg. Chem.* **1992**, *31*, 1550). The redox couples range from 1.59 to 0.96 V versus NHE and are believed to involve the tetraamidate ligand. The use of σ^+ (instead of σ) in the analysis suggests that delocalization is important in this redox process. The exceptionally large ρ value further supports the noninnocent character of the ligand. This in is contrast to the results obtained for the $[VO(depa-X)]^{2-}$ complexes, where the correlation for σ versus $E^{o\prime}$ is significantly better than that obtained for σ^+.
(31) Holmes, S.; Carrano, C. J. *Inorg. Chem.* **1991**, *30*, 1231.
(32) Borovik, A. S.; Raymond, K. N. To be submitted for publication.
(33) An irreversible oxidative wave is found for all the H_4depa-X ligands under the same voltammetric conditions. The $E_{p,a}$ values range from 1.28 to 1.64 V versus SCE.
(34) It is likely that a semiquinone-like species would have a significantly lower affinity for the VO^{3+} cation than $(depa-X)^{4-}$.
(35) Another plausible explanation is that the oxidation to the semiquinone state leads to filming of the electrode surface, which blocks the $VO^{3+/2+}$ electron transfer. We thank a reviewer for this suggestion.

ligand-based redox process ($E_{p,a}^{ox2}$ = 0.78 V) occur at relatively low potentials. This combination of Lewis donor strength and oxidative stability makes this family of ligands extraordinarily effective in stabilizing V(V) oxo species.

Summary. Metal oxo cations only exist for metal ions with highly oxidized metal centers.[36] As a consequence, all molecular systems designed to recognize these cations must contain a binding pocket that can stabilize the metal. We have developed a new ligand system H_4depa-X (where X = Me, H, Cl, NO_2), which contains a di[*N*-amidate–*O*-phenolate] metal-binding pocket. It was anticipated that the strong σ-donating ability of this binding pocket would lead to stable metal oxo complexes. The tetraanionic H_4depa-X ligands readily form oxovanadium(IV) complexes that are stable both in the solid state and solution. The $[VO(depa\text{-}X)]^{2-}$ complexes have been used to test the viability of the di[*N*-amidate–*O*-phenolate] unit as the metal binding core for metal oxo cation receptors. Infrared, electronic absorption, and EPR spectroscopies evince that the di[*N*-amidate–*O*-phenolate] donor set provides an extremely electron-rich environment about the vanadium(IV) center. Electrochemical studies reveal a near-reversible, diffusion-controlled VO^{3+}/VO^{2+} couple at potentials that are significantly lower than those found for other square pyramidal oxovanadium(IV) complexes. In addition, the potential of this redox couple can be tuned by a single substitution on the amidato–phenolato rings. The solid-state structure of $[VO(depa\text{-}H)]^{2-}$ shows that the ethyl groups of the propanediamido backbone span both faces of the vanadium–$(depa\text{-}H)^{4-}$ coordination plane, suggesting that the pendant arms are flexible enough to extend over the oxo moiety. These results demonstrate that the $(depa\text{-}X)^{4-}$ ligands can serve as the molecular foundation to support appended hydrogen-bond donors. Work toward this end is ongoing.

Acknowledgment is made to the National Science Foundation (Grant CHE-8919207) for support of this work. T.M.D. thanks the National Science Foundation for a graduate fellowship.

Supplementary Material Available: Anisotropic thermal parameters for non-hydrogen atoms (Table S1), a list of intramolecular angles and distances for $(depa\text{-}X)^{4-}$ (Table S2), and final hydrogen atom positions (Table S3) (3 pages). Ordering information is given on any current masthead page.

(36) Holm, R. H. *Chem. Rev.* **1987**, *87*, 1401.